Available online at www.sciencedirect.com

ScienceDirect

MATTER AND RADIATION AT EXTREMES

Matter and Radiation at Extremes 2 (2017) 287–295

www.journals.elsevier.com/matter-and-radiation-at-extremes

Research Article

Transport properties of warm and hot dense iron from orbital free and corrected Yukawa potential molecular dynamics

H.Y. Sun [a,b], Dongdong Kang [b], Yong Hou [b], J.Y. Dai [b,*]

[a] *Northwest Institute of Nuclear Technology, Xi'an, Shaanxi 710024, PR China*
[b] *Department of Physics, College of Science, National University of Defense Technology, Changsha, Hunan 410073, PR China*

Received 20 January 2017; revised 4 September 2017; accepted 11 September 2017
Available online 12 October 2017

Abstract

The equation of states, diffusions, and viscosities of strongly coupled Fe at 80 and 240 eV with densities from 1.6 to 40 g/cm^3 are studied by orbital-free molecular dynamics, classical molecular dynamics with a corrected Yukawa potential and compared with the results from average atom model. A new local pseudopotential is generated for orbital free calculations. For low densities, the Yukawa model captures the correct ionic interaction behavior around the first peak of the radial distribution function (RDF), thus it gives correct RDFs and transport coefficients. For higher densities, the scaled transformation of the Yukawa potential or adding a short range repulsion part to the Yukawa potential can give correct RDFs and transport coefficients. The corrected potentials are further validated by the force matching method.

PACS codes: 34.20.Cf; 52.25.Fi; 52.27.Gr; 52.65.Yy

Keywords: Transport properties; Orbital-free molecular dynamics; Yukawa model; Force matching

1. Introduction

The equation of states and transport properties of warm dense matter (WDM) and hot dense matter (HDM) are essential in experiments and theories, for their applications in the models of giant planet core [1,2], in the design and analysis of shock compression experiments [3–6], and their roles in comparison and validation of the models in describing WDM and HDM. The widely used density functional theory (DFT) based first-principles molecular dynamics (FPMD) methods in calculating the WDM are considered reliable to obtain such properties, but are restrained by the computational costs, especially for large systems where many plane waves are needed, or at high temperatures where lots of bands are needed. The fast developing orbital-free (OF) methods [7–12] reduce the computational costs, but they work well only for high temperatures or simple elements currently [7,16]. Another important branch of methods starts from solving the electronic structure of one atom, and the variable interactions of adjacent ions on the electronic structure are neglected or taken into account by an external potential with spherical symmetry [17–19]. To study the ionic structures and transport properties, the electronic structures of a single atom can be used for constructing the ion–ion pair potential, then molecular dynamics are carried out with this pair potential, such as average atom molecular dynamics (AAMD) [17] or pseudo-atom molecular dynamics (PAMD) [22,23]. The hyper-netted chain (HNC) approximation within the Ornstein-Zernike (OZ) equation can also be solved to describe the ionic

* Corresponding author.
E-mail address: jydai@nudt.edu.cn (J.Y. Dai).

Peer review under responsibility of Science and Technology Information Center, China Academy of Engineering Physics.

https://doi.org/10.1016/j.mre.2017.09.001

structure if the ion–ion pair potential is obtained [17,24–26], which can be used to calculate the electronic and ionic structures and the X-ray Thomson scattering (XRTS) spectrum in the WDM regime [27]. Based on the electronic structures of one atom, these methods are efficient and can give the quantities such as the ionization degree and shell structure, but their behaviors for the strongly coupled systems should always be checked carefully. Using the 'atomic scale' methods, such as molecular dynamics combining Yukawa model, to complement the orbital-free molecular dynamics (OFMD) calculations, can restate the results from the atomic view and benchmark the model itself in the related region [20,21].

Warm dense Fe attracts a lot of attention for its existence in Earth interior [28,29], terrestrial planets and exoplanets, and its common usage in experiments [6] and calculations. X-ray diffraction experiments [30] and calculations with FPMD [31–33] and molecular dynamics based on embedded atom method [34,35] have been used to study the melting boundary of warm dense Fe in the Earth core. Lots of calculations on compressed Fe have been carried out, such as equation of states by FPMD [36,37], OFMD [7,38], and average atom (AA) molecular dynamics model [17], and transport properties by FPMD [40,41]; but few about the structures at high temperature are announced because of the complex electronic structures of Fe and expensive computational costs. Recently, Bailey's experiment [42] shows that even for Fe at about 180 eV and 0.4 g/cm^3, the measured opacity is 30–400% larger than the results of the atomic models. Therefore, the properties of Fe below the solid density, especially the role of the surrounding ions on the atomic structures, should be studied carefully. FPMD or OFMD is the most popular method to study the local environments but few calculations were carried out for the Fe below solid density, especially for the temperature higher than 100 eV. Essentially, FPMD or OFMD calculations solve the electronic structure in the potential of all ions, thus they can provide another way to make comparisons with the atomic models, for the environmental effects of ions included reasonably. Yukawa potential is usually used in the study of strongly coupled plasmas, which can give good computational efficiency and ionic structures [3,20,21]. However, whether it is valid for warm dense matter in a wide temperature and density range is also required to check.

In this work, both OFMD and classical molecular dynamics (CMD) with Yukawa potentials are used to study the structure and transport properties of Fe at 80 and 240 eV from 1.6 to 40 g/cm^3, where the Yukawa model works well at low densities and becomes invalid as the density increases. Results of AA model are also included. The interatomic potentials are focused, and the correction of the Yukawa model is further validated by force matching method. The relation with the interatomic potentials and the transport properties are also discussed.

2. Calculation methods

2.1. Orbital-free molecular dynamics

In DFT, the electronic free energy functional has the form:

$$F^{\mathrm{e}}[n(\boldsymbol{r})] = F^{0}[n] + \frac{1}{2}\int\int \mathrm{d}\boldsymbol{r}\mathrm{d}\boldsymbol{r}'\frac{n(\boldsymbol{r})n(\boldsymbol{r}')}{|\boldsymbol{r}-\boldsymbol{r}'|} + \int n(\boldsymbol{r})v(\boldsymbol{r})\mathrm{d}\boldsymbol{r} + \int f_{\mathrm{xc}}[n]\mathrm{d}\boldsymbol{r}, \tag{1}$$

where n denotes the electron density, $F^0[n]$ is the kinetic energy functional, $v(\boldsymbol{r})$ is the external potential, $f_{\mathrm{xc}}[n]$ is the exchange-correlation functional. The OF method means the expression of $F^0[n]$ does not depend on the electron orbital explicitly. In Thomas-Fermi framework, $F^0[n]$ can be written as [7,44],

$$F^{0}[n] = \frac{1}{\beta}\int \mathrm{d}\boldsymbol{r}\left[\boldsymbol{n}(\boldsymbol{r})\boldsymbol{\Phi}(\boldsymbol{n}(\boldsymbol{r}))-\frac{\boldsymbol{2\sqrt{2}}}{\boldsymbol{3\pi^2\beta^{3/2}}}\boldsymbol{I_{3/2}}\boldsymbol{\Phi}(\boldsymbol{n}(\boldsymbol{r}))\right], \tag{2}$$

where $\beta=1/kT$, k is the Boltzmann constant. $\Phi(n(\boldsymbol{r}))$ is defined by:

$$n(\boldsymbol{r}) = \frac{\sqrt{2}}{\pi^2\beta^{3/2}}I_{1/2}[\Phi(n(\boldsymbol{r}))], \tag{3}$$

where $I_v(x)$ is Fermi integral,

$$I_v(x) = \frac{1}{\Gamma(v+1)}\int \frac{t^v}{1+\mathrm{e}^{t-x}}\mathrm{d}t, \tag{4}$$

and $\Gamma(v)$ is Gamma function.

For orbital free density functional calculation, the local pseudopotential is required, and its generation is of great challenge [45]. The local pseudopotential is generated using the method in Lambert's work [7]. The electron density $\rho(r)$ is firstly solved in the cell model [46], then regularized to $\tilde{\rho}(r)$ inside a cutoff radius r_{c}:

$$\tilde{\rho}(r) = \begin{cases} \dfrac{1}{4\pi}\exp\left(a+br^2+cr^4\right) & r<r_{\mathrm{c}} \\ \rho(r) & r\geq r_{\mathrm{c}} \end{cases}, \tag{5}$$

where a, b, c are determined by equal the values of $\tilde{\rho}(r_{\mathrm{c}})$, $\partial\tilde{\rho}(r)/\partial r|_{r=r_{\mathrm{c}}}$, $\int_0^{r_{\mathrm{c}}}\tilde{\rho}(r)\mathrm{d}r$ with those of $\rho(r)$. The pseudopotential is obtained by

$$\tilde{\phi}(r) = \mu - \frac{1}{\beta}I_{1/2}^{-1}\left(\frac{\pi^2\beta^{3/2}}{\sqrt{2}}\tilde{\rho}(r)\right) - \int \mathrm{d}\boldsymbol{r}'\frac{\tilde{\rho}(\boldsymbol{r}')}{|\boldsymbol{r}-\boldsymbol{r}'|}, \tag{6}$$

where μ is the chemical potential. The pseudopotentials generated at different temperatures and densities only have small difference in their values, and the used pseudopotential is generated at 7.9 g/cm^3 and 80 eV with a cutoff radius of 0.8 atomic units (a.u.). It should be noted that this local pseudopotential includes full electrons in the valence.

The ABINIT program [47,48] is used to perform OFMD calculations. The local density approximation exchange-correlation functional is applied. The electron wave functions are expanded into plane waves up to a cutoff energy of 100 Hartree, where the total energy and pressure converge within 0.01%. The OF method in this work tends to

overestimate the pressure and only exhibits well for Fe at very high temperatures [43,52,54]. The FP calculations with the 22 valence electrons PAW pseudopotential have been carried out on some 32 atoms structures at 40 g/cm^3 and 80 eV, and comparisons show that, in our OF calculations, the overestimation of the pressure is within 5%. Another validation is the comparison with the SESAME EOS # 2140 Hugoniot line at the temperature of 100 eV, and the calculated pressure and diffusion coefficients are also consistent with the previous results [38,39] at 22.5 g/cm^3, 10 eV and 34.5 g/cm^3, 100 eV. The pressures and radial distribution functions (RDF) are also consistent with our previous FP results [37].

For the following OF results in this work, 108 atoms are included in the simulation cell with periodic boundary conditions, and tests on larger systems do not show apparent change on RDFs and diffusions. The Gaussian thermostat [50] is used in the simulation and the initial structure is face-centered cubic (fcc) crystal. The velocity autocorrelation function is used to estimate the correlation time τ, and the results in the initial 40τ are discarded to ensure the system is in thermal equilibration. Then simulations last for 1−6 ps, with time steps of 0.1−0.2 fs, for different densities and temperatures.

2.2. Yukawa model

In Yukawa model [13,14], the static potential $V(\boldsymbol{r})$ related charge density $\rho(\boldsymbol{r})$ is given by Poisson's equation:

$$\Delta V(\boldsymbol{r}) = -\frac{\rho(\boldsymbol{r})}{\varepsilon_0}. \tag{7}$$

With the Fermi-Dirac distribution, the total, bound, free electron densities $n_\mathrm{e}(\boldsymbol{r})$, $n_\mathrm{eb}(\boldsymbol{r})$, $n_\mathrm{ef}(\boldsymbol{r})$ at temperature T and position $\boldsymbol{r}$ are:

$$\int\limits_{\varepsilon_k\geq 0} \frac{1}{\mathrm{e}^{\frac{\varepsilon_k+q_\mathrm{e}V(\boldsymbol{r})-\mu}{kT}}+1} g(\varepsilon)\mathrm{d}\varepsilon = n_\mathrm{e}(\boldsymbol{r}), \tag{8}$$

$$\int\limits_{\varepsilon_k=0}^{\varepsilon_k+q_\mathrm{e}V(\boldsymbol{r})=0} \frac{1}{\mathrm{e}^{\frac{\varepsilon_k+q_\mathrm{e}V(\boldsymbol{r})-\mu}{kT}}+1} g(\varepsilon)\mathrm{d}\varepsilon = n_\mathrm{eb}(\boldsymbol{r}), \tag{9}$$

$$\int\limits_{\varepsilon_k+q_\mathrm{e}V(\boldsymbol{r})\geq 0} \frac{1}{\mathrm{e}^{\frac{\varepsilon_k+q_\mathrm{e}V(\boldsymbol{r})-\mu}{kT}}+1} g(\varepsilon)\mathrm{d}\varepsilon = n_\mathrm{ef}(\boldsymbol{r}), \tag{10}$$

where μ is the chemical potential, $q_\mathrm{e} = -e$ is the electron charge, $\varepsilon_k = p^2/2m$, $g(\varepsilon)$ is the degeneracy of the electron orbital, and free electron degeneracy $g(\varepsilon) = 2/(2\pi)^2 (2m/\hbar^2)^{3/2}\varepsilon_k^{1/2}$ is used in the calculation. The average free electron density $\overline{n}_\mathrm{ef}$ is given by the electron density at $\lim\limits_{r\to\infty} V_\mathrm{e}(\boldsymbol{r}) = 0$.

For an ion in the polarized electron background, the charge density is $\rho(\boldsymbol{r}) = Z_\mathrm{ion}\delta(\boldsymbol{r}) - en_\mathrm{e}(\boldsymbol{r}) + e\overline{n}_\mathrm{e}$. Using the linear approximation $n_\mathrm{e}(\boldsymbol{r}) \approx \overline{n}_\mathrm{e} + V_\mathrm{e}(\boldsymbol{r})\partial n_\mathrm{e}(\boldsymbol{r})/\partial V_\mathrm{e}(\boldsymbol{r})$, the solution of the Poisson's equation becomes

$$V(\boldsymbol{r}) = \frac{1}{4\pi\varepsilon_0}\frac{Z_\mathrm{ion}}{r}\mathrm{e}^{-k_y r}, \tag{11}$$

where $k_y = \sqrt{\frac{q_\mathrm{e}^2\overline{n}_\mathrm{e}}{\varepsilon_0 kT}\frac{I_{-1/2}(\mu/kT)}{I_{1/2}(\mu/kT)}}$ is the screening parameter [15,38]. And the interatomic potential between Z_i charge particle and Z_j charge particle in the polarized electron background is:

$$V_{ij}(\boldsymbol{r}) = \frac{1}{4\pi\varepsilon_0}\frac{Z_i Z_j}{r}\mathrm{e}^{-k_y r}. \tag{12}$$

The chemical potential μ can be obtained by solving Eq. (8) and Eq. (11). The number of the bound electrons in $V(\boldsymbol{r})$ is $n_\mathrm{eb} = \int_V n_\mathrm{eb}(\boldsymbol{r})\mathrm{d}\boldsymbol{r}$, and it should equal $Z_\mathrm{ion} - \overline{n}_\mathrm{ef}/n_i = Z_\mathrm{ion} - Z_\mathrm{I}$, where $Z_\mathrm{I} \triangleq \overline{n}_\mathrm{ef}/n_i$ is the average ionization degree. Taking a trial ionization degree and solving the equations iteratively can get μ and $\overline{n}_\mathrm{ef}$ finally.

The interatomic potential in Eq. (12) is used for the CMD simulation. 864 atoms are used in the simulation cell and the initial structure is fcc. The time steps are 0.1−0.2 fs for different cases and the simulations last for 10^5 time steps after thermal equilibration.

2.3. Calculation of diffusion and viscosity

The diffusion and viscosity of the ions can be obtained by the Green-Kubo formula [40,51,53]:

$$D = \lim_{t\to+\infty} D_\mathrm{GK}(t), \tag{13}$$

$$D_\mathrm{GK}(t) = \frac{1}{3N}\sum_{i=1}^{N}\int_0^t \langle v_i(\tau)v_i(0)\rangle \mathrm{d}\tau, \tag{14}$$

$$\eta = \lim_{t\to+\infty} \eta_\mathrm{GK}(t), \tag{15}$$

$$\eta_\mathrm{GK}(t) = \frac{1}{3VkT}\sum_{\alpha>\beta}\int_0^t \langle \sigma_{\alpha\beta}(\tau)\sigma_{\alpha\beta}(0)\rangle \mathrm{d}\tau, \tag{16}$$

$$\sigma_{\alpha\beta}(\tau) = \sum_{i=1}^{N} m_i v_{i\alpha}(t)v_{i\beta}(t) + \sum_{i=1}^{N} r_{i\alpha}(t)f_{i\beta}(t), \tag{17}$$

where i is the index of the ion, α, β represent the three directions x, y, and z, $\langle\rangle$ for the ensemble average. V is the volume of the simulates system, k is the Boltzmann constant, T is the temperature, and f is the force on the ion. The diffusion coefficients are sensitive to the size of the system [40,53], and our tests show that 108 atoms can give convergent results. The viscosity does not show apparent dependence on the system size, but it requires a long time simulation to decrease the fluctuations [53].

3. Results and discussion

3.1. Average ionization degree and equation of state

The Yukawa model is used here within the density of 0.4–40 g/cm^3 at 80, 120, 180, and 240 eV, whose related parameters are listed in Table 1. The coupling parameter is the ratio between the interatomic potential and the kinetic energy, and the corresponding values in Table 1 show that the systems are in strong coupling. Γ_c is much larger than Γ_y, which shows the essential role of screening. Here, $\Gamma_c = \frac{1}{1.5kT}\frac{Z_I Z_I}{r_{WS}}$ and $\Gamma_y = \frac{e^{-r_{WS}k_y}}{1.5kT}\frac{Z_I Z_I}{r_{WS}}$ (r_{WS} is the Wigner-Seitz radius $\frac{4}{3}\pi r_{WS}^3 = \frac{V}{N}$). The average ionization degrees are further plotted in Fig. 1, which increase with increasing temperature, for more electrons are excited above the zero energy at a higher temperature. Along the isothermal line, the average ionization degrees decrease with density first, and then increase. Two effects contribute to this behavior: (1) When the ionization degree is fixed, increasing the ion density equals to increasing the free electron density. Larger free electron density indicates higher electron chemical potential at $V = 0$, so that the free electron tends to fill the $V \neq 0$ region, which induces the decrease of the ionization degree. (2) Increasing the electron density means to increase the screening parameter, so that the potential becomes shallower. It should be easier for the electrons to escape from the shallower ion potential to become free, which will increase the ionization degree. Also, there is a competition between the density effect and temperature effect. At higher temperature, electrons will be ionized easier.

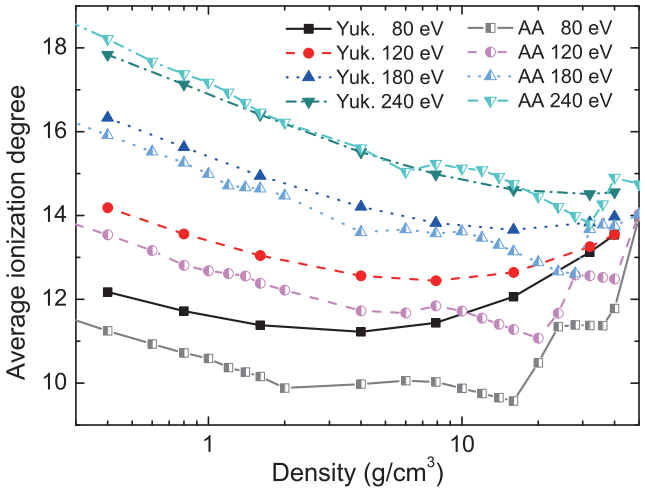

Fig. 1. The average ionization degree obtained in the Yukawa model (filled symbols) and the AA model (half filled symbols) along the isothermal line.

Table 1
The average ionization degree Z_I, screening parameter k_y, coupling parameter $\Gamma_c = \frac{1}{1.5kT}\frac{Z_I Z_I}{r_{WS}}$ and $\Gamma_y = \frac{e^{-r_{WS}k_y}}{1.5kT}\frac{Z_I Z_I}{r_{WS}}$ obtained in the Yukawa model.

ρ (g/cm^3)	T (eV)	Z_I	k_y (1/bohr)	r_{WS}	Γ_c	Γ_y
0.4	80	12.2	0.182	7.20	7.00	1.89
0.4	120	14.2	0.161	7.20	6.34	1.99
0.4	180	16.3	0.141	7.20	5.60	2.03
0.4	240	17.8	0.127	7.20	5.01	2.00
0.8	80	11.7	0.252	5.72	8.17	1.94
0.8	120	13.6	0.222	5.72	7.29	2.05
0.8	180	15.6	0.195	5.72	6.46	2.13
0.8	240	17.1	0.176	5.72	5.82	2.12
1.6	80	11.4	0.350	4.54	9.71	1.99
1.6	120	13.0	0.307	4.54	8.50	2.11
1.6	180	14.9	0.269	4.54	7.44	2.20
1.6	240	16.4	0.244	4.54	6.72	2.22
4.0	80	11.2	0.543	3.34	12.82	2.09
4.0	120	12.6	0.473	3.34	10.70	2.20
4.0	180	14.2	0.412	3.34	9.13	2.30
4.0	240	15.5	0.374	3.34	8.16	2.34
7.9	80	11.4	0.756	2.66	16.70	2.23
7.9	120	12.4	0.654	2.66	13.18	2.31
7.9	180	13.8	0.568	2.66	10.84	2.39
7.9	240	15.0	0.514	2.66	9.55	2.43
16	80	12.1	1.062	2.11	23.51	2.51
16	120	12.6	0.916	2.11	17.20	2.50
16	180	13.7	0.792	2.11	13.39	2.53
16	240	14.6	0.716	2.11	11.49	2.55
32	80	13.1	1.452	1.67	35.06	3.10
32	120	13.3	1.268	1.67	23.83	2.86
32	180	13.8	1.098	1.67	17.30	2.76
32	240	14.5	0.990	1.67	14.29	2.73
40	80	13.5	1.591	1.55	40.19	3.40
40	120	13.5	1.402	1.55	26.81	3.05
40	180	14.0	1.218	1.55	19.02	2.88
40	240	14.6	1.099	1.55	15.48	2.82

To check the parameters of Yukawa model, the average ionization degrees of the AA model are shown in Fig. 1. In the AA model used here, the electron orbitals are obtained by solving the Dirac equation with a mean central potential $V(r)$ inside the Wigner-Seitz sphere. The central potential $V(r)$ includes the Coulomb, exchange, and correlation interactions between the electrons and the nuclear potential $-Ze^2/r$, where the interactions between the electrons are expressed by the electron density $\rho(r)$. The electron density is obtained by the Fermi-Dirac distribution on the electron orbitals, and these quantities are solved self-consistently [26,55]. The AA model here differs from the Yukawa model in solving the electron orbitals and including the exchange and correlation effects, and it can be seen as more reasonable. At 80 eV, the Yukawa model overestimates the average ionization degrees for about 1 for all the densities below 7.9 g/cm^3. The overestimation decreases with increasing temperature, and vanishes at 240 eV. The reason is that, at high temperatures, high energy electrons are the main part of the ionized electrons, and they are analogous to be free electrons. Therefore AA model and Yukawa model give consistent average ionization degree. An obvious manner of the AA average ionization degree is the oscillation along the isothermal line. The oscillations may be caused by the atomic shell structure, and their values are small below the solid density (7.9 g/cm^3).

The equation of states is shown in Fig. 2. Note that the pressure obtained in the CMD simulations with Yukawa potential of Eq. (12) does not include the contributions from free electrons. The pressure of the free electron can be evaluated by the Fermi gas model:

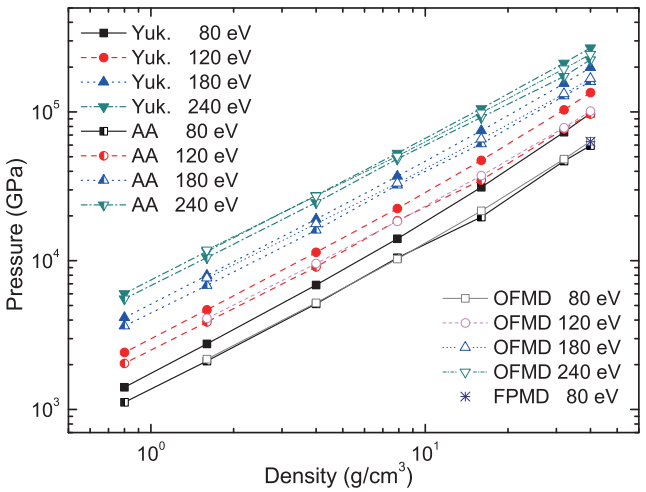

Fig. 2. The pressures obtained by OFMD (open symbols) calculations, Yukawa (filled symbols) and AA (half filled symbols) models. The result of FPMD at 80 eV and 40 g/cm^3 is shown by the cross symbol. The Hartwigsen-Goedecker-Hutter pseudopotential with 16 electrons is used in the FP calculation [49]. The 32-atom cubic cell is used in the FPMD, and the simulation lasts for 1.6 ps with a time step of 0.2 fs.

$$P_{\mathrm{f}} = \frac{1}{\pi^2}\int_0^{\infty} \frac{\frac{1}{3}p^2 \times p^2 \mathrm{d}p}{1+\exp[(p^2/2-\mu)/kT]} = \left(2^{3/2}/3\pi^2\right)T^{5/2}I_{3/2}(\mu/kT). \quad (18)$$

This expression does not include the exchange contribution which has a negative contribution to the pressure, and the bond effect is neglected. Therefore, the total pressure from CMD with Yukawa potential can be overestimated by 5%–30% compared with OFMD results. The pressures from the AA model can be in good agreement with OFMD here, since the orbital effects are not important in the conditions considered here.

3.2. RDFs and potential corrections

RDFs are the basic structural properties to show the two body spatial correlations, and are usually used to compare the calculations with pair potentials and the results of FPMD or OFMD [7,52,56,57]. The calculated RDFs are shown in Fig. 3. At 80 eV, for 1.6 and 4.0 g/cm^3, the Yukawa model and OFMD give consistent results (The RDFs of the Yukawa model is slightly steeper than the OFMD's, but this difference can disappear if we use the ionization degrees from the AA model into the Yukawa potential), while the difference increases with the density and temperature. At higher densities or temperatures, in comparison with the RDFs of OFMD, the first peak of the RDFs from the Yukawa model is shifted towards zero position, and the height of the first peak is also lower. It indicates the underestimation of the ionic interactions at short distances, and this underestimation is also found in the previous comparisons [52,56,57]. When the electronic cloud around one ion starts to overlap with the other, the repulsed interaction rises due to the Pauli exclusion principle. This effect dominates the repulsion behavior at short distance, and it is not included in the Yukawa model. Adding a short-range repulsion (SRR) term to the ionic interaction potential can correct this defect [52,56,58], and one simple but restrained [59] example is as follows

$$V_{\mathrm{Yuk.}}^{\mathrm{SRR}}(r) = \frac{a}{r^4} + \frac{1}{4\pi\varepsilon_0}\frac{Z_{\mathrm{ion}}^2 e^2}{r}\mathrm{e}^{-k_y r}, \quad (19)$$

where the r^{-4} behavior is obtained by fitting methods [56,58], the parameter a relates to the radial extension of the ions, and it only changes with the ionization degree [56]. The values of a can be fitted by comparing the calculated forces or RDFs with the referenced results [57]. Here the values of a are fitted by comparing the RDFs with the results of OFMD. The RDFs at 80 eV obtained by different a are shown in Fig. 4 (a). Apparent modifications are found at 40 g/cm^3, and the same a values have less influence on the RDFs at 1.6 g/cm^3. At 1.6 g/cm^3, the position reaching to the peak of the RDF is large, thus the contributions of the SRR term is small due to the r^{-4} behavior. The fitted a parameters decrease with increasing density and increase with increasing temperature.

The comparisons of the forces are shown in Fig. 5, where the OF results are taken as reference. The moduli (Fig. 5(a)) of

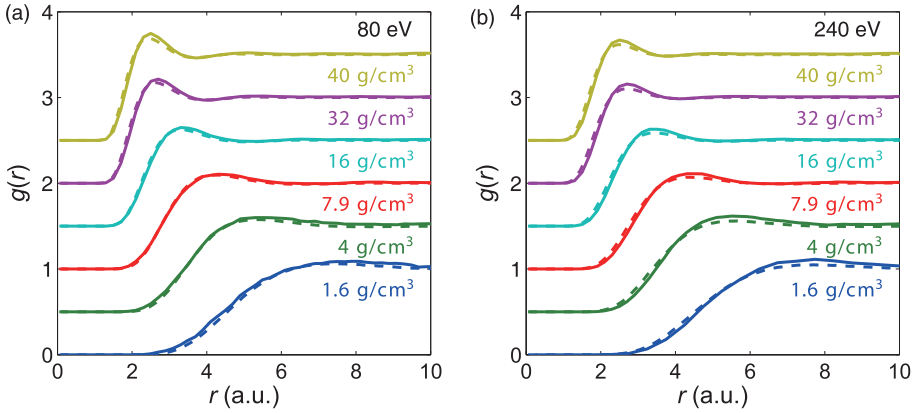

Fig. 3. The RDFs at (a) 80 eV and (b) 240 eV. The solid lines are the results of OFMD, and the dash ones are the results of Yukawa model. The RDFs of 4.0–40 g/cm^3 are upshifted by 0.5, 1.0, 1.5, 2.0, and 2.5, respectively.

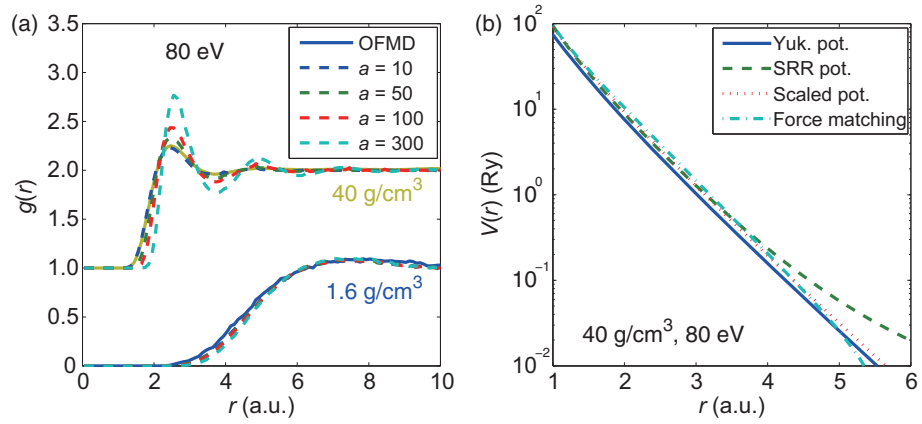

Fig. 4. (a) shows the SRR RDFs with different parameter a's at 80 eV. The RDFs of 40 g/cm^3 upshift by 1. (b) shows the different pair potentials at 80 eV and 40 g/cm^3. The results of Yukawa potential, SRR potential, scaled Yukawa potential, and potential obtained by force matching method are labeled by 'Yuk. pot.', 'SRR pot.', 'scaled pot.', 'force matching', respectively.

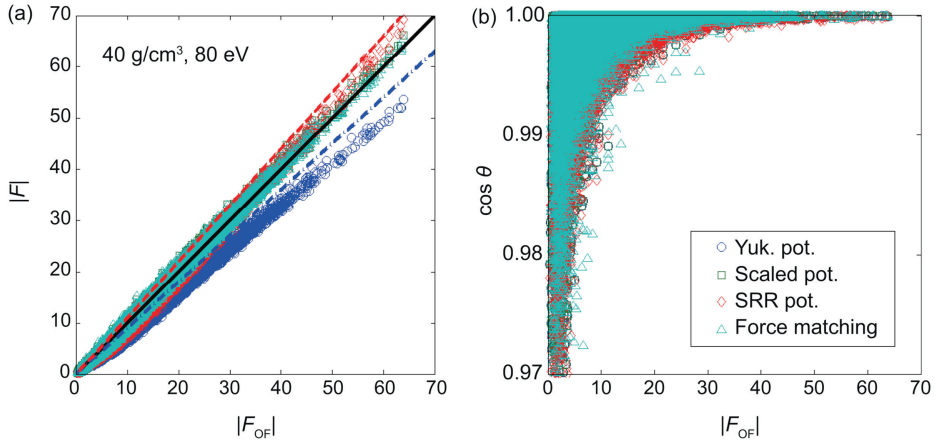

Fig. 5. The force comparison using the forces of OF calculations as the benchmark at 80 eV and 40 g/cm^3. The x value is set to be the modulus of the OF force in a.u. (a) shows the modulus of the force from different potentials (the labels are the same as in Fig. 4), and the dash-dot, solid and dash lines mean $0.9|F_{\rm OF}|$, $|F_{\rm OF}|$ and $1.1|F_{\rm OF}|$, respectively, where $|\ |$ means the modulus of the force vector. (b) shows the cosine value of the angle between the pair potential force and the OF force, $\cos\theta = |F_{\rm OF}\cdot F_y|/(|F_{\rm OF}||F_y|)$, where y is one of the pair potentials.

the Yukawa force are around a straight line and most of the cosine values of the angle between the force (Fig. 5(b)) are bigger than 0.99, except for the small forces. So scaling the potential [60] is a feasible method to give the proper forces and RDFs:

$$V_{\rm scale}(r) = C(\rho,T)V_{\rm Yuk.}(r), \tag{20}$$

where the multiplied factor $C(\rho,T)$ takes the form $C(\rho,T) = c_0(T) + c(T)\rho$ with $c_0(T) = 0.85$, 0.96, 1.1, 1.2, and $c(T) = 0.01$, 0.007, 0.004, 0.001 cm$^3\cdot$g^{-1} for 80, 120, 180, and 240 eV. The RDFs of the corrected potentials and the OFMD's RDFs are nearly the same and indistinguishable, and the improved RDFs are not shown in Fig. 3.

The above two corrected methods give different potential behaviors as shown in Fig. 4(b). Whether there should be a 'uniform' and 'correct' interatomic potential is an interesting project. The effective pair interactions can be extracted from the OFMD force using the force matching method [58,61]. Here, piecewise cubic splines are used to construct the form that the force modulus changes with the distance r. The distance is divided into M sections with dividing point r_k, $k = 1$, 2, …, $M+1$, and for $r \in [r_k, r_{k+1}]$, the force is represented as:

$$\begin{aligned} F_k(r) = {} & \frac{1}{6}\frac{\Delta_k\Delta_{k+1}}{d_k}[(d_k-\Delta_{k+1})K_k + (d_k+\Delta_k)K_{k+1}] \\ & -\frac{\Delta_{k+1}}{d_k}y_k + \frac{\Delta_k}{d_k}y_{k+1}, \end{aligned} \tag{21}$$

where $d_k = r_{k+1} - r_k$, $\Delta_k = r - r_k$, $\Delta_{k+1} = r - r_{k+1}$; y_k and y_{k+1} are values of $F(r)$ at r_k, r_{k+1}; K_k and K_{k+1} are values of $\mathrm{d}^2F(r)/\mathrm{d}r^2$ at r_k, r_{k+1}. y_k and K_k are the parameters, and the force of ith atom gives a series of 3 linear equations:

$$\boldsymbol{F} = \sum_j \boldsymbol{F}_{\rm pair}(\boldsymbol{r}_{ji}) = \sum_j F_{\rm pair}(r_{ji})\boldsymbol{r}_{ij}/r_{ji}, \tag{22}$$

where the summation of j is for all atoms inside the cutoff sphere of the ith atom. The least square method is used to solve the linear equations, where the 'global minimum' is

obtained, and tests with model potentials show that this method reconstructs the input potentials with high precision.

For 32 g/cm^3 and 80 eV, the cutoff radius is set to be 10 a.u. and a radial grid with an interval of 0.05 at [0.6, 2.0] and an interval of 0.1 at [2.0, 10] is used in the fitting program. The potential is obtained by integrating the force value from the cutoff radius to 0. There are limited samples at $r < 1.2$, where the value of the fitted force has fluctuations or 0 values. The potential in this region is set to $V(r) = c_1/r + c_2$ with c_1 and c_2 obtained by fitting the potential at [1.2, 1.3]. The obtained pair potential from OFMD calculations is shown in Fig. 4(b). It exhibits the same behaviors around the first peak of RDF (Fig. 4(a)) as the scaled and SRR potentials. The tail behavior of scaled Yukawa potential is consistent with the potential obtained by force matching method, which shows the validation of the scaled method. The comparisons of the forces between the pair potential by force matching and OF calculations are presented in Fig. 5. Most of the errors in the modulus (Fig. 5(a)) are within 10% (the dash-dot and the dash lines), and most of the cosine values (Fig. 5(b)) are within 0.99. The departures are more apparent for smaller forces, and these differences should be attributed to the many-body interactions beyond pair styles.

The RDFs are mainly determined by the interactions around the first peak of the RDF. It is usual to compare the RDFs to validate the coupling parameters [7,62] and average ionization degree [63]. This should be careful for the densities above the solid density, where the electrostatic interaction becomes invalid as the density increases.

3.3. Transport coefficients

The obtained diffusion coefficients are shown in Fig. 6. The diffusion coefficients increase with increasing temperatures and decrease with increasing densities, which is in agreement with the common sense that ions escape from their local environment faster at the conditions of higher kinetic energy and weaker interactions. The Yukawa model underestimates

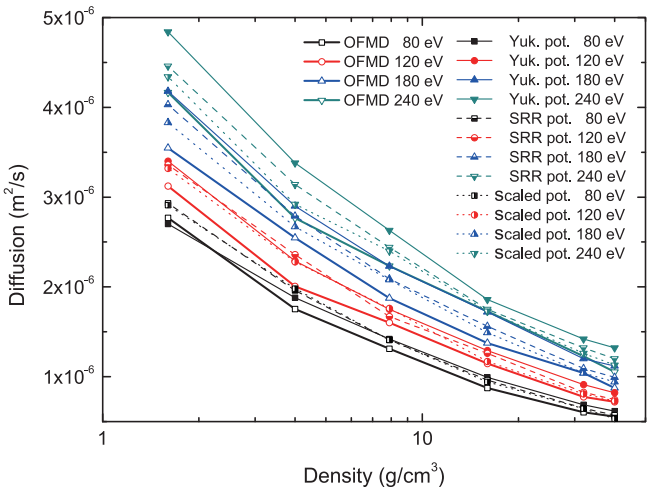

Fig. 6. The diffusion coefficients obtained by OFMD and classical molecular dynamics with Yukawa potential.

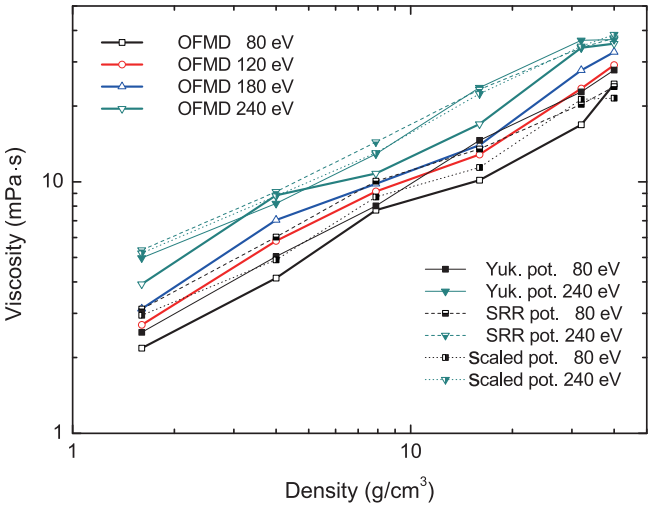

Fig. 7. The viscosity coefficients obtained by OFMD and classical molecular dynamics. The results of classical molecular dynamics are shown only for 80 and 240 eV.

the interactions at high densities, so that the corresponding diffusions are overestimated. Comparing with the results of OFMD, the scaled potentials give consistent diffusion coefficients in the whole density region. The agreement shows that, in the strongly coupled region, short range repulsion plays a dominant role in deciding the diffusion coefficients. The contribution to the force from the long range behavior of the potential may be counteracted by the nearly uniform angular distribution of the ions at long distances, and has little effect on the diffusion coefficients. Note that the diffusions from OFMD are smaller than the pair potentials, which is caused by the many-body interactions also.

The calculated viscosities are shown in Fig. 7. There are some fluctuations along the isothermal line, which is caused by the statistical errors. The viscosities increase with increasing density and temperature (though the change with temperature is not apparent) for both the CMD and OFMD calculations. In comparison with the OFMD results, the CMD results do not have system errors, and the corrected potentials do not improve the agreement apparently.

4. Conclusion

The structural and transport properties of Fe at 80 and 240 eV with densities from 1.6 to 40 g/cm^3 are calculated by OFMD and CMD with Yukawa potentials. New local pseudopotential is generated for the OFMD calculations. The Yukawa model added by pressure from Fermi electron gas overestimates the pressure by 5%–30% for the lack of exchange and bond effects. The Yukawa model works well for relatively low densities, where the ionization degrees are consistent with the results of AA model and the obtained ionic forces and RDFs agree well with those from OFMD. When the density increases above the solid density (7.9 g/cm^3), the ionic coupling become larger, and the overlaps of the electron wave functions from adjacent ions become important. In this region, the Yukawa potentials can be corrected by scaling or adding

SRR term to give correct RDFs and diffusion coefficients, where the key modification is the potential's behaviors around the location of RDF's first peak. The application of force matching method with pair potential checks the validation of the Yukawa potential form, and shows the ability of pair potential in describing the interactions between ions.

Acknowledgments

This work is supported by the National Basic Research Program of China (973 Program) under grant no. 2013CB922203, the National NSFC under grant Nos. 11422432 and 11774429, Science Challenge Project under grant no. JCKY2016212A501, and the Advanced Research Foundation of National University of Defense Technology under grant no. JQ14-02-01. Calculations were carried out at the Research Center of Supercomputing Application, National University of Defense Technology.

References

[1] V.V. Brazhkin, A.G. Lyapin, Universal viscosity growth in metallic melts at megabar pressures: the vitreous state of the Earth's inner core, Phys. Usp. 43 (2000) 493−508.
[2] G.A. de Wijs, G. Kresse, L. Vočadlo, D. Dobson, D. Alfè, et al., The viscosity of liquid iron at the physical conditions of the Earth's core, Nature 392 (1998) 805.
[3] M.S. Murillo, Viscosity estimates of liquid metals and warm dense matter using the Yukawa reference system, High Energy Density Phys. 4 (2008) 49−57.
[4] D. Galmiche, S. Gauthier, On the Reynolds number in laser experiments, Jpn. J. Appl. Phys. 35 (1996) 4516.
[5] T. Desai, H.C. Pant, Control of Rayleigh-Taylor instabilities in laser accelerated seeded targets, Laser Part. Beams 18 (2000) 119.
[6] Y. Ping, F. Coppari, D.G. Hicks, B. Yaakobi, D.E. Fratanduono, et al., Solid iron compressed up to 560 GPa, Phys. Rev. Lett. 111 (2013) 065501.
[7] F. Lambert, J. Clérouin, G. Zérah, Very-high-temperature molecular dynamics, Phys. Rev. E 73 (2006) 016403.
[8] H. Chen, A. Zhou, Orbital-free density functional theory for molecular structure calculations, Numer. Math. Theor. Meth. Appl. 1 (2008) 1−28.
[9] V.V. Karasiev, T. Sjostrom, S.B. Trickey, Generalized-gradient-approximation noninteracting free-energy functionals for orbital-free density functional calculations, Phys. Rev. B 86 (2012) 115101.
[10] V.V. Karasiev, D. Chakraborty, O.A. Shukruto, S.B. Trickey, Nonempirical generalized gradient approximation free-energy functional for orbital-free simulations, Phys. Rev. B 88 (2013) 161108.
[11] T. Sjostrom, J. Daligault, Fast and accurate quantum molecular dynamics of dense plasmas across temperature regimes, Phys. Rev. Lett. 113 (2014) 155006.
[12] V.V. Karasiev, T. Sjostrom, J. Dufty, S.B. Trickey, Accurate homogeneous electron gas exchange-correlation free energy for local spin-density calculations, Phys. Rev. Lett. 112 (2014) 076403.
[13] S. Hamaguchi, R.T. Farouki, Thermodynamics of strongly coupled Yukawa systems near the one component plasma limit. I. Derivation of the excess energy, J. Chem. Phys. 101 (1994) 9876−9884.
[14] D. Chattopadhyay, H.J. Queisser, Electron scattering by ionized impurities in semiconductors, Rev. Mod. Phys. 53 (1981) 745−768.
[15] H. Siegfried, Glenzer, Ronald Redmer, X-ray Thomson scattering in high energy density plasmas, Rev. Mod. Phys. 81 (2009) 1625−1663.
[16] V.V. Karasiev, T. Sjostrom, S.B. Trickey, Finite-temperature orbital-free DFT molecular dynamics: coupling Profess and Quantum Espresso, Comput. Phys. Commun. 185 (2014) 3240−3249.
[17] Y. Hou, J. Yuan, Alternative ion-ion pair-potential model applied to molecular dynamics simulations of hot and dense plasmas: Al and Fe as examples, Phys. Rev. E 79 (2009) 016402.
[18] S. Kiyokawa, Multi-average ion model for hot dense plasmas derived from finite temperature density-functional theory, High Energy Density Phys. 13 (2014) 40−54.
[19] C. Gao, J. Zeng, J. Yuan, Plasma screening effects on the atomic structure and radiative opacity of dense carbon plasmas based on the DLA model, High Energy Density Phys. 7 (2011) 54−60.
[20] J.D. Kress, J.S. Cohen, D.P. Kilcrease, D.A. Horner, L.A. Collin, Orbital-free molecular dynamics simulations of transport properties in dense-plasma uranium, High Energy Density Phys. 7 (2011) 155−160.
[21] M. Marciante, M.S. Murillo, Thermodynamic and kinetic properties of shocks in two-dimensional Yukawa systems, Phys. Rev. Lett. 118 (2011) 025001.
[22] C.E. Starrett, D. Saumon, Equation of state of dense plasmas with pseudoatom molecular dynamics, Phys. Rev. E 93 (2016) 063206.
[23] C.E. Starrett, J. Daligault, D. Saumon, Pseudoatom molecular dynamics, Phys. Rev. E 91 (2015) 013104.
[24] K. Wünsch, P. Hilse, M. Schlanges, D.O. Gericke, Structure of strongly coupled multicomponent plasmas, Phys. Rev. E 77 (2008) 056404.
[25] V. Bezkrovniy, M. Schlanges, D. Kremp, W.D. Kraeft, Reaction ensemble Monte Carlo technique and hypernetted chain approximation study of dense hydrogen, Phys. Rev. E 69 (2004) 061204.
[26] Y. Hou, F. Jin, J. Yuan, Energy level broadening effect on the equation of state of hot dense Al and Au plasma, J. Phys. Condens. Matter 19 (2007) 425204.
[27] Y. Hou, R. Bredow, J. Yuan, R. Redmer, Average-atom model combined with the hypernetted chain approximation applied to warm dense matter, Phys. Rev. E 91 (2015) 033144.
[28] J.P. Poirier, Light elements in the Earth's outer core: a critical review, Phys. Earth Planet. Inter. 85 (1994) 319.
[29] T. Lay, J. Hernlund, B.A. Buffett, Core-mantle boundary heat flow, Nat. Geosci. 1 (2008) 25−32.
[30] S. Anzellini, A. Dewaele, M. Mezouar, P. Loubeyre, G. Morard, Melting of iron at Earth's inner core boundary based on fast X-ray diffraction, Science 340 (6131) (2013) 464−466.
[31] D. Alfè, G.D. Price, M.J. Gillan, Iron under Earth's core conditions: liquid-state thermodynamics and high-pressure melting curve from ab initio calculations, Phys. Rev. B 65 (2002) 165118.
[32] D. Alfè, M.J. Gillan, G.D. Price, Ab initio chemical potentials of solid and liquid solutions and the chemistry of the Earth's core, J. Chem. Phys. 14 (2002) 6170.
[33] J. Bouchet, S. Mazevet, G. Morard, F. Guyot, R. Musella, Ab initio equation of state of iron up to 1500 GPa, Phys. Rev. B 87 (2013) 094102.
[34] Q. Cao, P. Wang, D. Huang, J. Yang, M. Wan, et al., Transport coefficients and entropy-scaling law in liquid iron up to Earth-core pressures, J. Chem. Phys. 140 (2014) 114505.
[35] F. Luo, Y. Cheng, X. Chen, L. Cai, F. Jing, The melting curves and entropy of iron under high pressure, J. Chem. Eng. Data 56 (2011) 2063−2070.
[36] J. Dai, Y. Hou, J. Yuan, Unified first principles description from warm dense matter to ideal ionized gas plasma: electron-ion induced friction, Phys. Rev. Lett. 104 (2010) 245001.
[37] J. Dai, D. Kang, Z. Zhao, Y. Wu, J. Yuan, Dynamic ionic clusters with flowing electron bubbles from warm to hot dense iron along the Hugoniot curve, Phys. Rev. Lett. 109 (2012) 175701.
[38] D. Gilles, F. Lambert, J. Clérouin, G. Salin, Yukawa monte carlo and orbital free molecular dynamics approaches for the equation of state and structural properties of hot dense matter, High Energy Density Phys. 3 (2007) 95−98.
[39] F. Lambert, J. Clérouin, S. Mazevet, Structural and dynamical properties of hot dense matter by a Thomas-Fermi-Dirac molecular dynamics, Europhys. Lett. 75 (2006) 681−687.
[40] J. Dai, Y. Hou, D. Kang, H. Sun, J. Wu, et al., Structure, equation of state, diffusion and viscosity of warm dense Fe under the conditions of giant planet core, New J. Phys. 45 (2013) 045003.

[41] C. Wang, Z.B. Wang, Q.F. Chen, P. Zhang, Quantum molecular dynamics study of warm dense iron, Phys. Rev. E 89 (2014) 023101.
[42] J.E. Bailey, T. Nagayama, G.P. Loisel, G.A. Rochau, C. Blancard, et al., A higher-than-predicted measurement of iron opacity at solar interior temperatures, Nature 517 (2015) 56−59.
[43] F. Lambert, V. Recoules, A. Decoster, J. Clérouin, M. Desjarlais, On the transport coefficients of hydrogen in the inertial confinement fusion regime, Phys. Plasmas 18 (2011) 056306.
[44] R.P. Feynman, N. Metropolis, E. Teller, Equations of state of elements based on the generalized Fermi-Thomas theory, Phys. Rev. 75 (1949) 1561−1573.
[45] C. Huang, E.A. Carter, Transferable local pseudopotentials for magnesium, aluminum and silicon, Phys. Chem. Chem. Phys. 10 (2008) 7109.
[46] W.R. Johnson, FORTRAN Program for Temperature-dependent Thomas-Fermi Atom, 2002. http://www.nd.edu/johnson/.
[47] X. Gonze, J.M. Beuken, R. Caracas, F. Detraux, M. Fuchs, et al., First-principles computation of material properties: the ABINIT software project, Comput. Mater. Sci. 25 (2002) 478−492.
[48] X. Gonze, G. Rignanese, M. Verstraete, J. Beuken, Y. Pouillon, et al., A brief introduction to the ABINIT software package, Z. Krist. 220 (2005) 558−562.
[49] C. Hartwigsen, S. Goedecker, J. Hutter, Relativistic separable dual-space Gaussian pseudopotentials from H to Rn, Phys. Rev. B 58 (1998) 3641−3662. The energy cutoff is set to be 100 Hartree and *Gamma* point is used in the sampling of the Brillouin zone. It is necessary to check whether the 16 electrons pseudopotential is transferrable at 40 g/cm^3 and 80 eV. Some structures extracted from the molecular dynamics are calculated using a 22 electrons PAW pseudopotential, and the difference in the pressure between the two sets is about 5%.
[50] F. Zhang, Operator-splitting integrators for constant-temperature molecular dynamics, J. Chem. Phys. 06 (1997) 6102−6106.
[51] M.P. Allen, D.J. Tildesley, Molecular Simulation of Liquids, Oxford Science Publications, Oxford, 1987.
[52] T.G. White, S. Richardson, B.J.B. Crowley, L.K. Pattison, J.W.O. Harris, et al., Orbital-free density-functional theory simulations of the dynamic structure factor of warm dense aluminum, Phys. Rev. Lett. 111 (2013) 175002.
[53] J.F. Danel, L. Kazandjian, G. Zérah, Numerical convergence of the self-diffusion coefficient and viscosity obtained with Thomas-Fermi-Dirac molecular dynamics, Phys. Rev. E 85 (2012) 066701.
[54] F. Lambert, J. Clérouin, S. Mazevet, D. Gilles, Properties of hot dense plasmas by orbital-free molecular dynamics, Contrib. Plasma Phys. 47 (2007) 272−280.
[55] Y. Hou, F. Jin, J. Yuan, Influence of the electronic energy level broadening on the ionization of atoms in hot and dense plasmas: an average atom model demonstration, Phys. Plasmas 13 (2006) 093301.
[56] K. Wünsch, J. Vorberger, D.O. Gericke, Ion structure in warm dense matter: benchmarking solutions of hypernetted-chain equations by first-principle simulations, Phys. Rev. E 79 (2009) 010201 (R).
[57] J. Vorberger, D.O. Gericke, Effective ion-ion potentials in warm dense matter, High Energy Density Phys. 9 (2013) 178−186.
[58] S. Izvekov, M. Parinello, C.J. Burnham, G.A. Voth, Effective force fields for condensed phase systems from ab initio molecular dynamics simulation: a new method for force-matching, J. Chem. Phys. 120 (2004) 10896−10913.
[59] The a/r^4 SRR term has a disadvantage that it cannot be Fourier-transformed which restricts some applications such as the derivation of local field corrections, and a modified type is provided in J. Vorberger, D. O. Gericke, Effective ion-ion potentials in warm dense matter, High Energy Density Phys. 9 (2013) 178−186.
[60] H. Sun, D. Kang, J. Dai, W. Ma, L. Zhou, et al., First-principles study on equation of states and electronic structures of shock compressed Ar up to warm dense regime, J. Chem. Phys. 144 (2016) 124503.
[61] F. Ercolessi, J.B. Adams, Interatomic potentials from first-principles calculations, Europhys. Lett. 26 (8) (1994) 583−588.
[62] T. Ott, M. Bonitz, L. Stanton, M.S. Murillo, Coupling strength in Coulomb and Yukawa one-component plasmas, Phys. Plasmas 21 (2014) 113704.
[63] M.S. Murillo, J. Weisheit, S.B. Hansen, M.W.C. Dharma-wardana, Partial ionization in dense plasmas: comparisons among average-atom density functional models, Phys. Rev. E 87 (2013) 063113.